International Journal of Biological Macromolecules 268 (2024) 131676

Contents lists available at ScienceDirect

International Journal of Biological Macromolecules

journal homepage: www.elsevier.com/locate/ijbiomac

Green synthesis of chitosan- and fluoride-functionalized silver nanoparticles using *Camellia sinensis*: Characterization and dental applications

Carolina Cifuentes-Jiménez [a,*], María Victoria Bolaños-Carmona [b], Tattiana Enrich-Essvein [a], Alejandro B. Rodríguez-Navarro [c], Santiago González-López [a], Monica Yamauti [d], Pedro Álvarez-Lloret [e,*]

[a] Department of Operative Dentistry, School of Dentistry, University of Granada, Spain
[b] Department of Pediatric Dentistry, School of Dentistry, University of Granada, Spain
[c] Department of Mineralogy and Petrology, Faculty of Sciences, University of Granada, Spain
[d] Department of Restorative Dentistry, Graduate School of Dental Medicine, Hokkaido University, Japan
[e] Department of Geology, Faculty of Geology, University of Oviedo, Spain

ARTICLE INFO

Keywords:
Silver nanoparticles
Plant extract
Green chemistry technology
Tooth remineralisation
Dentine

ABSTRACT

The development of new biocompatible and eco-friendly materials is essential for the future of dental practice, especially for the management of dental caries. In this study, a novel and simple method was applied for the green synthesis of silver nanoparticles (AgNPs) from the aqueous extract of *Camellia sinensis* (WT) and functionalized with chitosan (CHS) and NaF. The effects of WT_AgNPs application on demineralized dentin were evaluated for potential dental applications. The WT_AgNPs showed molecular groups related to organic compounds, potentially acting as reducing and capping agents. All AgNPs presented spherical shapes with crystal sizes of approximately 20 nm. Forty human molars were assigned to control: sound (SD) and demineralised dentine (DD), and experimental groups: WT_AgNPs, WT_AgNPs_NaF, and WT_AgNPs_CHS. Then, the NPs were applied to DD to evaluate the chemical, crystallographic, and microstructural characteristics of treated-dentine. In addition, a three-point bending test was employed to assess mechanical response. The application of WT_AgNPs indicated a higher mineralisation degree and crystallites sizes of hydroxyapatite than the DD group. SEM images showed that WT_AgNPs presented different degrees of aggregation and distribution patterns. The dentine flexural strength was significantly increased in all WT_AgNPs. The application of WT_AgNPs demonstrated remineralising and strengthening potential on demineralised dentine.

1. Introduction

The use of silver as an antibacterial agent dates to ancient Western civilizations. In past Medicine, silver salts were utilized in different applications as antibacterial and antimycotic agents, for example to treat mental diseases or in the treatment of burns and wounds. Several of those silver-based drugs are still prescribed and distributed, but others have been improved, and novel applications have been introduced [1]. Dentistry has benefited from the advances in silver-based compounds, as observed in the successful use of silver fluoride to manage dental caries [2], which consists of a biofilm-mediated, diet-modulated, multifactorial, non-communicable, dynamic disease resulting in net mineral loss of dental hard tissue. Caries management and control consist of different strategies that interfere with mineral loss during the different stages of the disease [3]. Different approaches, such as non-invasive or micro-invasive strategies and restorative/invasive interventions, are necessary to manage the wide range of caries processes and lesions. The non-invasive approach requires control of diet and biofilm and promotion of hard tissue mineralisation. The use of sealants as a barrier against acid diffusion into susceptible tooth surfaces and resin infiltration of initial enamel lesions are successful micro-invasive approaches. Contrarily, invasive caries management entails the removal of irreversibly demineralised tissues and the placing of a restorative material. However, despite the continuous evolution of dental materials, dental caries

* Corresponding authors.
E-mail addresses: carolinaccj@correo.ugr.es (C. Cifuentes-Jiménez), pedroalvarez@uniovi.es (P. Álvarez-Lloret).

https://doi.org/10.1016/j.ijbiomac.2024.131676
Received 10 December 2023; Received in revised form 6 April 2024; Accepted 16 April 2024
Available online 17 April 2024

continues to be a remaining chronic disease in our society, which ultimately causes tooth loss [2].

Fluorides play a fundamental role in the prevention of dental caries and are also used therapeutically for the inactivation of incipient carious lesions [4]. The presence of fluoride ions in the apatite and/or dissolution prevent the extensive dissolution of dental apatite crystals while enhances the precipitation of (F- and OH-) apatite crystals, which are more resistant against acid dissolution in the caries process [5]. Thus, fluoride is able to promote remineralization of tooth structures by accelerating the growth of new fluorapatite crystals by bringing calcium and phosphate ions, as well as inhibiting the activity of carious bacteria [6]. Sodium fluoride (NaF) is a highly bioavailable active component widely used in toothpaste, mouthwashes, and water fluoridation [7].

Nanotechnology has enabled the development of silver nanoparticles (AgNPs), aiming at their antibacterial effects, such as AgNPs functionalised with fluoride (fluoride-AgNPs) [8]. Fluoride-AgNPs showed low toxicity to living cells and high antibacterial capacity against *Streptococcus mutans* [9–11]. The mechanism of fluoride-metal NPs formation involves a combination of reduction, stabilization and surface functionalization [12]. These fluorine-functionalised NPs exhibit enhanced chemical reactivity and dispersibility (inhibiting NPs aggregation), making the nanoparticles potentially suitable for various technological and biomedical applications (e.g. catalysis, biomedical imaging and drug delivery) [12,13].

There are multiple methods for synthesizing silver nanoparticles, including physical and chemical reduction [14,15]. However, these approaches tend to be costly and labor-intensive, involving the use of toxic reagents such as sodium dodecyl and sodium citrate. Additionally, these procedures consume significant energy and contribute to pollution and public health concerns [16,17]. With the increasing utilization of silver nanoparticles, particularly in health sciences, seeking alternative, cost-effective, and environmentally friendly synthesis methods becomes a social imperative [18]. The utilization of plant extracts has emerged as a promising solution due to their simplicity, safety, low cost, rapid reaction times, and effectiveness in producing AgNPs [17,19]. Green chemistry explores the potential of plants, algae, bacteria, and fungi for AgNP synthesis [14,17]. These nanoparticles are formed through the oxidation of Ag^{+} to Ag^{0} by various biomolecules present in plants, such as flavonoids, ketones, aldehydes, tannins, carboxylic acids, phenolics, and proteins [20]. Different plant extracts from a variety of species (i.e. *Azadirachta indica*, *Thymus kotschyanus*, *Cyanthillium cinereum*) have been successfully employed in synthesizing silver nanoparticles, including tea extracts [17,21].

White tea (*Camellia sinensis*, WT) has gained popularity and prominence in this context due to its minimal processing and numerous health benefits [21]. Obtained from buds and young leaves, WT retains high concentrations of catechins [22], including epigallocatechin-3-gallate (EGCG), known for its antioxidant, antimicrobial, antidiabetic, anti-inflammatory, and cancer-preventive. EGCG is particularly effective against oral bacteria, such as *Streptococcus mutans* [23]. The EGCG from WT also exhibits an inhibitory activity on collagenases that degrade the organic matrix, generating collagen stability and improving the mechanical properties of the tooth [24]. In addition, the phenolic hydroxyls in the EGCG enhance its potential to reduce Ag^{+} into Ag^{0} [21].

Following a similar environment-friendly approach, chitosan (CHS), a natural biopolymer, has also attracted great interest for its biomedical applications (i.e., antibacterial, antioxidant, chelating, and biopharmaceutical properties) [25,26]. Moreover, the high charge density of CHS and its ability to form complexes through electrostatic interactions with metal ions play a key role in the stabilization, reduction, shape orientation and size control of metal-NPs [27]. Previous studies have revealed that CHS can act as both reducing and stabilising agents for the synthesis of metal-NPs (e.g., AgNPs [28], CuNPs [29], and AuNPs [30]). Chitosan-functionalised AgNPs have shown antibacterial and antifungal potential [31]. In Dentistry, CHS has been widely investigated to develop biomaterials in restorative dentistry, implant dentistry, endodontics and periodontics [32–34].

Developing new biocompatible and nature-compatible materials is essential for the future of dental practice, especially in managing the most prevalent oral disease worldwide, caries. Considering the enormous potential of plants to act as reducing sources for AgNP, this research focused on applying a green biological technique to synthesize silver nanoparticles as an alternative to conventional methods, adding other compounds that may also enhance dentin remineralization. Hence, the present research aimed to (1) synthesize and characterize chitosan/NaF functionalised silver nanoparticles reduced with white tea (*Camellia sinensis*) and (2) evaluate the effects of WT_AgNPs application on demineralised dentin. The null hypotheses tested were (1) it would not be possible to synthesize AgNPs from *Camellia sinensis* extract and (2) WT_AgNPs application would not affect demineralised dentin.

2. Materials and methods

2.1. Synthesis of the silver nanoparticles (AgNPs)

AgNPs were synthesised following the protocol proposed by Zargar et al. [35]; 1 g of white tea (*Camellia sinensis*) supplied at Granadiet Herbalist (Granadiet, lot no. 224; Ogíjares, Spain) was added to 200 ml of ultrapure deionised MilliQ water (resistivity 18.2 M. Ω.cm, Millipore, Merck, Burlington, MA, USA), and then the solution was heated at 75 °C for 1 h under 350 rpm stirring. Then, the supernatant was vacuum-filtered (WP6111560; Merck Millipore, Billerica, MA, USA) using #3 filter paper (Ahlstrom, Stockholm, Sweden). Subsequently, 200 ml of silver nitrate ($AgNO_3$) 0.1 M were mixed with 200 ml of the previous white tea extract and maintained under 350 rpm stirring for 48 h at room temperature. The formation of AgNPs with white tea (WT_AgNPs) was monitored and determined by a color change from yellow to black (i.e., crystal precipitation). Finally, the solution obtained was centrifuged, and the NPs were washed with MilliQ water three times before drying for 24 h at 37 °C in the oven. The following functionalisation protocols were performed using the synthesised WT_AgNPs:

WT_AgNPs functionalised with chitosan (WT_AgNPs_CHS): 50 mg of chitosan was diluted in a 20 ml solution of 0.1 M acetic acid (CH_3COOH). Subsequently, chitosan preparation was dropped into 100 ml of WT_AgNPs solution at room temperature under stirring for 1 h [36].

WT_AgNPs functionalised with NaF (WT_AgNPs_NaF): 0.0571 g of sodium fluoride (NaF) was added into 100 ml WT_AgNPs of solution at room temperature under stirring for 24 h [37].

After WT_AgNPs functionalisation, both solutions were centrifuged, and the precipitates were washed with MilliQ water three times before drying for 24 h at 37 °C. All chemical reactants (≥99.0 % pure) were provided by Sigma-Aldrich (Sigma-Aldrich Chemicals; Saint Louis, MO, USA).

2.2. Characterisation of the AgNPs

Chemical characterisation was performed by infrared spectroscopy (ATR-FTIR: Jasco 6200; Easton, MD, USA) and thermogravimetric analysis (Mettler Toledo, TGA/DSC1 system; Schwarzenbach, Switzerland) to determine the molecular composition and the organic matter (%OM) content of the WT_AgNPs. Crystalline properties were determined by X-Ray Diffraction (XRD) analyses using X'Pert Pro diffractometer (PANalytical; Almelo, The Netherlands) and Transmission Electron Microscopy equipment (TEM: Carl Zeiss LIBRA 120 PLUS TEM; Jena, Germany, and HRTEM: JEOL JEM-2100F; Tokyo, Japan) equipments, to obtain crystallite size, crystal dimensions and degree of aggregation of the WT_AgNPs synthesised.

2.3. Dentine preparation

This study was approved by the Committee on Human and Animal Research (Reference number #1896–2020). Forty human molars without carious lesions or structural defects were stored in 0.1 % thymol solution at 4 °C. Tooth roots were separated from the crowns 2 mm below the cementum-enamel junction using an Isomet 11/1180 low-speed saw (Buehler; Lake Bluff, IL, USA) with a 456CA diamond disk (Struers; Copenhagen, Denmark) under copious irrigation. Teeth slices (9 mm in diameter × 1 mm in thickness) were acquired from transversal sections of the mid-coronal tooth. Subsequently, four beams (6 × 1 × 1 mm^3) were obtained from each tooth slice, resulting in 160 beams, and the enamel was removed by grounding with 600 grit silicon carbide papers. The dentin beams were rinsed and cleaned by ultrasonication for 30 min to remove the remaining debris. Then, all dentin beams were carefully examined under an optical microscope to confirm the absence of enamel, dentine microcracks or other imperfections.

The beams were randomly divided into two control groups: sound dentine (SD; $n = 32$) and demineralised dentine (DD; n = 32). Samples corresponding to the SD were stored at room temperature. The demineralised dentine was simulated using a pH-cycling procedure modified by Marquezan et al. [38]. All the specimens were immersed in 1 ml of a demineralising solution containing 2.2 mM $CaCl_2$, 2.2 mM NaH_2PO_4, and 50 mM acetic acid adjusted to a pH = 4.8 for 8 h. Subsequently, dentine beams were introduced in 1 ml of a remineralising solution containing 1.5 mM $CaCl_2$, 0.9 mM NaH_2PO_4, and 0.15 M KCl adjusted to a pH = 7.0 for 16 h. Chemical reagents (≥99.0 % purity) for solution preparation were supplied by Sigma-Aldrich (Sigma-Aldrich; Saint Louis, MO, USA). Each dentine beam was cycled for 14 days, and the solutions were renewed daily. The pH cycling was performed at room temperature without agitation. After the pH-cycling process, the beams corresponding to the DD were kept in storage. The remaining dentine beams were randomly divided according to the different AgNPs: WT_AgNPs, WT_AgNPs_CHS and WT_AgNPs_NaF ($n = 32$). Then, the dentine beams were treated with the three different WT_AgNPs for 5 min with a 0.5 % *v/w* in ultrapure deionised water under continuous stirring and then washed with distilled water for 1 min [39]. Finally, the beams were stored until further analysis.

2.4. Characterisation of AgNPs treated dentine specimens

2.4.1. Attenuated total reflectance infrared spectrometry (ATR-FTIR)

The beams ($n = 15$ per group) were analysed using a FTIR spectrometer (JASCO 6200, JASCO; Easton; MD, USA) equipped with a diamond-tipped ATR accessory (ATR Pro ONE, JASCO; Easton, MD, USA). Spectra were recorded in absorbance mode with a resolution of 2 cm^{-1} over 64 scan accumulations using a 400–4000 cm^{-1} in absorption mode. Overlapping peaks were resolved by a 2nd derivate method within each sectioned band using curve fitting PeakFit v4.12 software (Systat; San Jose, CA, USA). The degree of smoothing was set at 25 %, and the mixed Gaussian-Lorentzian function was employed for the peak area fitting. The curve fitting was accepted when r^2 achieved values higher than 0.95. From the peak area measurements, the following parameters were calculated: (1) Degree of mineralisation (band area ratio: v_1, v_3 PO_4^{3-}/Amide I): relative amount of phosphate mineral to the organic matrix (1640 cm^{-1} band) [40], and (2) Crystallinity index (CI): calculated as the ratio between the sub-bands areas at 1030 cm^{-1} (high crystalline apatite phosphates) to 1020 cm^{-1} (poorly crystalline apatite phosphates) within the v_1, v_3 PO_4^{3-} band region [41].

2.4.2. X-ray diffraction (XRD)

Two-dimensional X-ray diffraction (2D-XRD) patterns were obtained from one convenience sample per group using an X-ray diffractometer (Bruker D8 DISCOVER; Billerica, MA, USA) equipped with an area detector (DECTRIS PILATUS 3100 K-A; Baden, Switzerland). The XRD conditions were Cu Kα (λ = 1.5418 Å) radiation at 50 kV and 30 mA, with a pinhole collimator of 0.5 mm in diameter. The 2D-XRD patterns were registered at 2θ (Theta) scanning angle range from 20° to 60°, considering 19 steps and 40 s/step. The intensities concentrated in arcs within the Debye diffraction rings (corresponding to specific d-spacing/diffraction lines) were integrated to obtain a unidimensional scan (i.e., 2θ pattern). The crystallite size (*d*) of the hydroxyapatite (HAp) crystals was determined by measuring the full width at half maximum (FWHM) of the diffraction peak at 2θ position 25.9° (i.e., reflection line 002, corresponding to the c-axes direction). The Debye-Scherrer equation was employed for the *t* measurement:

$$t_{(002)} = \frac{K\lambda}{\beta \cos\theta}$$

where *t* is the average crystallite size (expressed in nm), λ corresponds to the wavelength of the X-ray source, K is the Scherrer constant (K = 0.89), and β is related to the FWHM of the line broadening for the (002) diffraction line.

2.4.3. Scanning electron microscopy (SEM)

One beam per group was randomly selected to study the different WT_AgNPs distribution on the dentine surface. The specimens were fixed in 2.5 % glutaraldehyde for 12 h at 4 °C. Then, the beams were immersed in a PBS solution for 1 h (20 min cycles) and rinsed in distilled water for 1 min. Subsequently, beams were dehydrated in ascending ethanol series (50 %, 70 %, 90 %, and 96 %). Finally, beams were mounted on aluminium stubs and carbon-coated using ion sputtering equipment (Hitachi UHS evaporator). Scanning electron microscopy (JSM-126610LV; JEOL; Japan) with an accelerating voltage of 10 kV and 10 mA was used to examine all specimens.

2.4.4. Mechanical test

Fifteen beams of each group were submitted to mechanical test to evaluate the dentine flexural properties. A universal testing machine (model Instron 3345; Instron, Canton, MA, USA) by a three-point bending test was employed using a 500 N load cell on a two-point support, with a length distance of 4.0 mm between points. The test was performed at a loading speed of 0.5 mm/min until the fracture of the dentine specimens.

2.4.5. Statistical analyses

Sample size estimation and power analysis for the experiments performed were carried out with the G*Power software (ver. 3.1.9.7; Heinrich-Heine-Universität Düsseldorf, Düsseldorf, Germany). The input parameters were as follows: two-tailed ANOVA power analyses test, 0.3 effect size d (medium), 0.05 α error level and 0.6 power (1-β error), indicating a minimum of 10 sample size per group. The mean and standard deviation were calculated for each parameter analysed. The variances homogeneity and the normality distribution were tested using the Levene and Shapiro-Wilk tests, respectively. The ATR-FTIR and flexural strength variables did not follow normal data distribution; non-parametric statistical tests were employed for these analyses. The Kruskal-Wallis test was used, followed by an intergroup analysis with the Mann-Whitney *U* test. A level of significance of $p < 0.05$ was established. Data were processed using SPSS statistical software (ver. 22; IBM, Armonk, NY, USA).

3. Results

3.1. Characterisation of AgNPs

The chemical composition of the samples was assessed by ATR-FTIR to determine the molecular components presented in the WT_AgNPs, and thermogravimetry analyses to obtain the organic matter content. The ATR-FTIR spectra of the different AgNPs are shown in Fig. 1. The WT_AgNPs (green line) and WT_AgNPs_NaF (blue line) spectra displayed

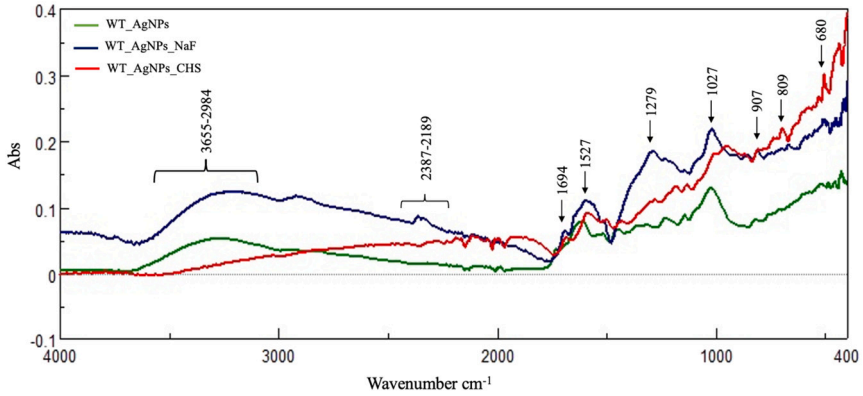

Fig. 1. Representative ATR-FTIR spectra of the different AgNPs obtained with white tea (WT) functionalised with chitosan CHS and NaF.

two broad bands at 3655–2984 cm^{-1} (associated with O—H stretching vibration, assigned to -OH group of polyols such as catechins) and 2387–2189 cm^{-1} (due to C—H stretching, aliphatic hydrocarbons) [42]. In addition, all the WT_AgNPs samples showed several peaks at 1694 cm^{-1} and 1279 cm^{-1} (C═C stretching, alkene groups), 1527 cm^{-1} and 907 cm^{-1} (C—N stretching vibrations, polyphenols and aliphatic amines), 1027 cm^{-1} (C═O stretching, ketones and quinones), and 809 cm^{-1} (C-O-C stretching, carboxylic acids and esters) [14]. These assignments are related to the molecular groups present in the organic components of the white tea used during the AgNPs synthesis [14,42]. On the other hand, the WT_AgNP_CHS (red line) spectra showed a peak at 680 cm^{-1}, revealing the presence of chitosan in the functionalisation of the AgNPs [43].

The main results obtained from thermogravimetry (TGA) analyses of the different WT_AgNPs heated from 25 °C to 600 °C using a heating rate of 10 °C/min under a nitrogen atmosphere are shown in Table 1. All WT_AgNPs showed similar weight loss percentages between 25 °C–130 °C due to adsorbed water, 130 °C–150 °C assigned to the polyphenols degradation of phytochemical compounds of the WT_AgNPs, and the loss up to 600 °C due to the thermal degradation of the resistant aromatic components of WT. Data from the TGA measurements revealed that WT_AgNPs and WT_AgNPs_NaF showed similar organic content (considering mass loss until 600 °C) with approximately 18 %, while WT_AgNPs_CHS was around 24 %.

The identification of the crystalline phases (silver nanoparticles) and their crystalline properties were determined by XRD analyses. The different WT_AgNPs showed XRD peaks at 38.2°, 44.3°, 64.5°, 77.5°, and 81.6° (2θ values) corresponding to Ag^0 face-centred cubic planes corresponding to (hkl) values - (111), (200), (220), (311) and (222) planes, respectively (labelled in Fig. 2). These results indicated the formation of silver colloidal crystals with a cubic structure in all NPs groups. The XRD pattern also revealed a lower intensity peak with a broad profile at 32.3°, corresponding to not fully reduced $AgNO_3$ particles in negligible amounts. Rietveld refinements of the XRD patterns reported the following cell parameters (considering Fm3 ¯m space group: JCPDS file no. 04–0783): a = 4.0845(1) Å for WT_AgNPs; a = 4.0841(1) Å for WT_AgNPs_CHS; and a = 4.0842(3) Å for WT_AgNPs_NaF. In addition, the Debye-Scherrer equation was employed to obtain the crystallite sizes (i.e., coherent crystal domains) for all nanoparticles: 19.10 nm, 20.57 nm, and 18.49 nm, respectively.

TEM observations were employed to determine the size and morphology of the different AgNPs, nanoparticles and their aggregation state, as well as the presence of organic coatings. Fig. 3 shows representative TEM images at different resolutions of the AgNPs synthesised. Nanoparticles presented spherical crystalline morphologies in all groups, showing a low percentage of aggregation mainly in WT_AgNPs and WT_AgNPs_CHS compared to WT_AgNPs_NaF (Fig. 3A–D vs G). In addition, all AgNPs were enveloped in a coating (gray color appearance) due to the presence of phytochemicals compounds like carbohydrates, flavonoids, glycosides, phenolic compounds, proteins, saponins, and tannins present in the white tea. High magnification TEM images (Fig. 3B–E–H) were used to obtain NPs crystal size averages: ~21 nm (WT_AgNPs), ~20 nm (WT_AgNPs-CHS), and ~ 19 nm (WT_AgNPs-NaF), which are in agreement with crystallite sizes determined by XRD. EDS elemental analyses of the previous images are shown in Fig. 3C–F–I, indicating representative Ag composition (i.e., 3 keV peak position in the spectrum).

Table 1
Organic matter content (O.M.%) obtained from the TGA analysis for the different WT_AgNPs. Values are expressed in mean ± SD.

AgNPs	O.M. (%)
WT_AgNPs	18.91 ± 1.21
WT_AgNPs_NaF	18.98 ± 0.62
WT_AgNPs_CHS	24.63 ± 0.12

3.2. Characterisation of WT_AgNPs application

3.2.1. Physico-chemical analyses of dentine

Table 2 presents the chemical composition of AgNPs determined by ATR-FTIR spectrometric analysis: Degree of mineralisation and Crystallinity Index (CI). Regarding the control groups, the Degree of mineralisation decreased in the demineralised dentine (DD) compared to sound dentine (SD). All applications with WT_AgNPs increased the degree of mineralisation in dentine reaching values comparable to the SD. In particular, the WT_AgNPs_NaF obtained the highest degree of mineralisation values between all experimental groups. On the other hand, the CI parameter increased for DD with respect to SD. In addition, the application of WT_AgNPs showed similar CI values between groups, although significantly higher in relation to SD groups and lower compared to DD. The hydroxyapatite (HAp) crystallite size (d) values after treatment with the different AgNPs synthesised are also summarised in Table 2. The results indicated a decrease in the crystallite size (i.e. crystalline domains for HAp) after the pH-cycling process (i.e., demineralised dentine) due to reduction of the size of apatite crystals during dissolution. However, after applying the different WT_AgNPs on the demineralised dentine, an increase in the crystallite size values was observed for all groups reaching values similar to SD.

3.2.2. Distribution of AgNPs on the dentine surface

Representative SEM images of the demineralised dentine treated with the different AgNPs are shown in Fig. 4. Spherical AgNPs were observed (i.e. bright spots) covering the dentine surfaces and partially filling the dentine tubules. The WT_AgNPs and WT_AgNPs_NaF groups (Fig. 4A and C, respectively) showed some degree of aggregation and a

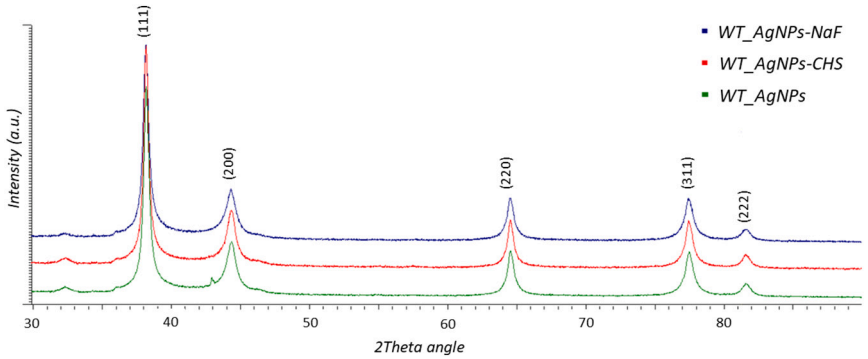

Fig. 2. Representative X-ray diffraction (XRD) patterns of the different AgNPs obtained with white tea (WT) functionalised with chitosan (CHS) and NaF. The Miller indices corresponding to each diffraction line are indicated in brackets (cubic structure).

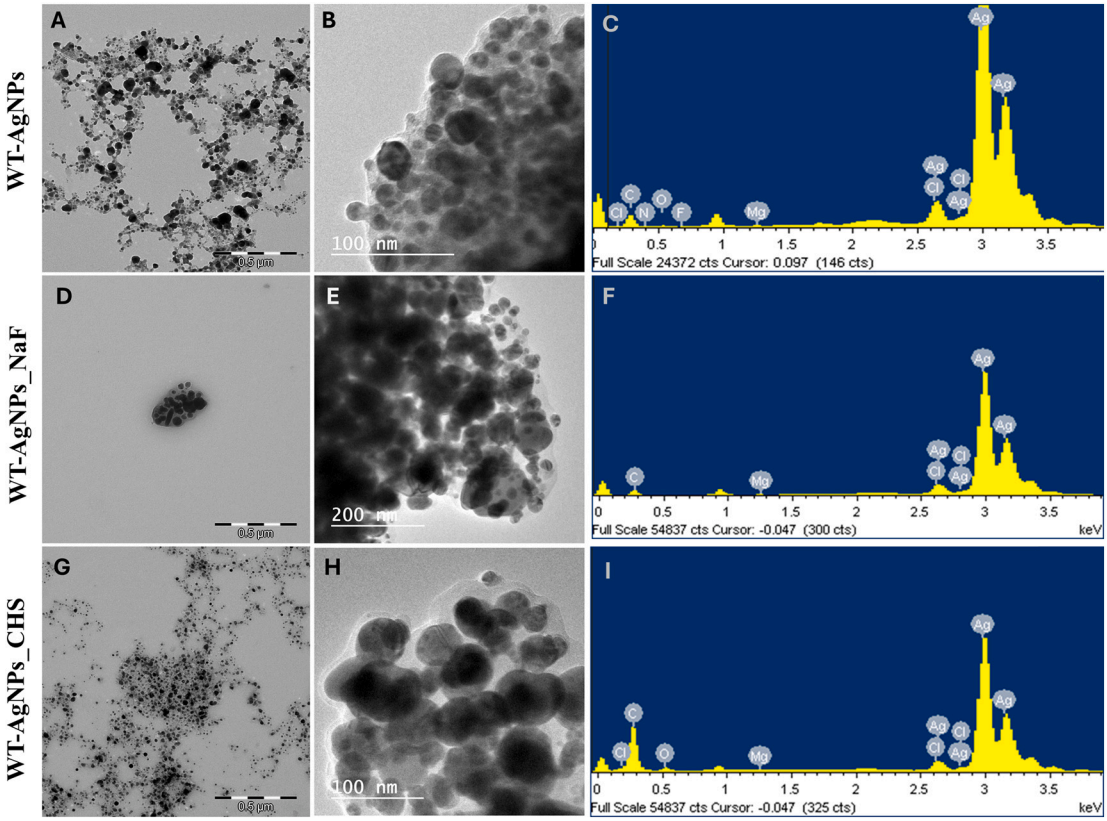

Fig. 3. Representative TEM images of NPs at different resolutions: WT_AgNPs (A–B), WT_AgNPs_CHS (D–E) and WT_AgNPs_NaF (G–H). Spectra represent elemental EDS analyses for each WT_AgNPs synthesised (C–F–I), indicating Ag composition (3 keV peak position).

Table 2
Compositional parameters and crystallinity of controls and experimental groups obtained by ATR-FTIR analysis: Degree of mineralisation and Crystallinity Index (CI). Crystallite size (*t*) values for hydroxyapatite crystals (HAp) of dentine samples obtained from the XRD analyses.

Experimental group	Degree of mineralisation	CI	*t* (nm)
Sound dentine (SD)	7.32 (0.66)[a]	0.48 (0.05)[a]	21.00
Demineralised dentine (DD)	3.85 (0.56)[b]	1.84 (0.35)[b]	12.60
WT_AgNPs	6.43 (0.46)[a]	0.75 (0.03)[c]	22.33
WT_AgNPs_NaF	8.83 (0.73)[c]	0.79 (0.03)[c]	21.66
WT_AgNPs_CHS	6.42 (0.63)[a]	0.85 (0.07)[c]	22.66

Values are expressed in mean (standard deviation). Different letters indicate significant differences between the groups (significance $p < 0.05$).

heterogeneous distribution on the surfaces, filling the tubules apertures. On the other hand, the WT_AgNPs_CHS (Fig. 4B) showed a more homogeneous distribution with a lower degree of aggregation on the surface of the demineralised dentine.

3.2.3. *Mechanical response of the dentine using different WT_AgNPs application*

The dentine flexural strength was obtained with three-point bending tests and showed significant differences in the mechanical properties as per different experimental groups (Fig. 5). The DD group had the lowest mechanical response values compared to those values of the SD group. The WT_AgNPs groups showed significantly higher values than DD ($p = 0.002$) and SD ($p = 0.003$) groups. No statistically significant differences were observed between the WT_AgNPs groups.

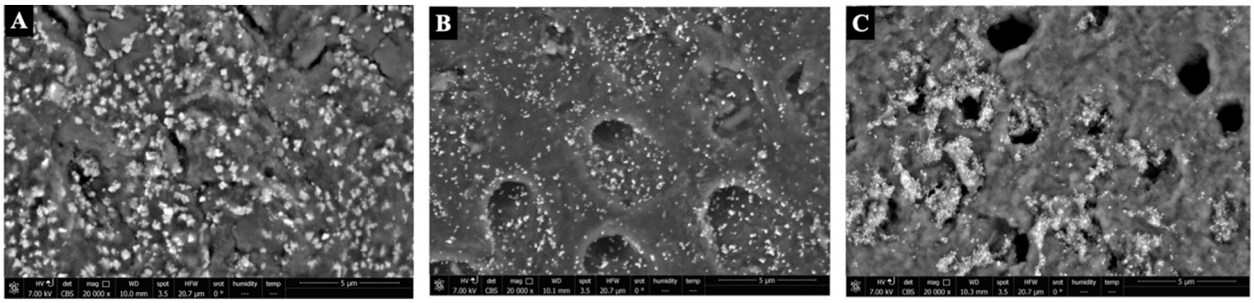

Fig. 4. Representative SEM images showing the AgNPs distribution in the demineralised dentine: (A) WT_AgNPs, (B) WT_AgNPs_CHS, (C) WT_AgNPs_NaF.

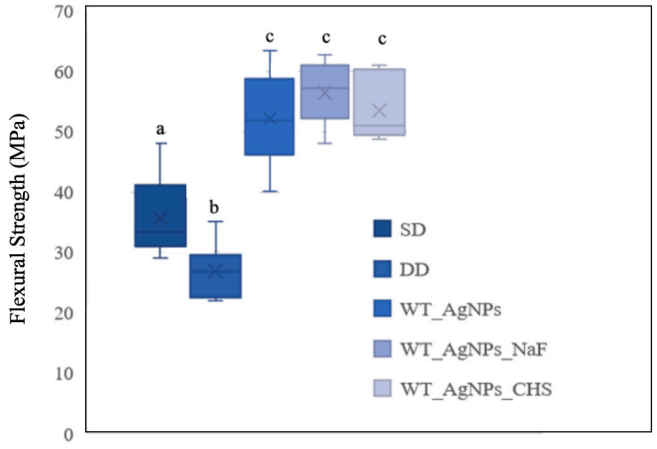

Fig. 5. Flexural strength of the dentine specimens for control groups (SD and DD) and WT_AgNPs groups was determined by a three-point bending mechanical test. Different letters indicate significant differences between groups ($p < 0.05$).

4. Discussion

The AgNPs synthesis by green chemistry is an efficient and reproducible method, offering interesting applications in dentistry. In this study, AgNPs reduced with white tea extract (*Camellia sinensis*) and functionalised with chitosan and NaF were successfully synthesised and applied to demineralised dentine to evaluate their restorative effects on the tooth substrate. The characterisation of the physicochemical properties of WT_AgNPs showed crystalline properties, different degree of aggregation and variable OM content related to the organic components employed during the green synthesis and functionalisation procedures. The results demonstrated that the WT_AgNP application in demineralised dentine significantly increased the degree of mineralisation and the crystallite size of the HAp, improving its mechanical properties. Therefore, the two null hypotheses of the present research had to be rejected. These WT_AgNPs obtained from plant extracts constitute an alternative to developing innovative products such as antimicrobial, antifouling, and remineralising agents that could be incorporated in different materials (e.g., root canal irrigants, mouthwashes, toothpastes, acrylic resins, adhesives or resin-based materials), enhancing the conventional dental practice.

Green chemistry offers an alternative to chemical and physical methods to synthesize silver nanoparticles employing organic compounds as stabilising and reducing agents [17]. The metal-NPs green synthesis from plant extracts involves three different phases: (1) the activation phase (i.e., bio-reduction of the metal salts and the nucleation process of reduced ions), (2) the growth phase, characterized by the spontaneous merging of small particles with larger ones through a process known as Ostwald ripening, and (3) the termination phase, which determines the final shape of the nanoparticles [44]. The use of plant extracts to synthesize metallic nanoparticles has shown various advantages, such as the simplicity of the procedure, low cost, and the absence of toxic substances [45]. In this process the presence of different biological components as reducing agents (e.g. flavones, terpenoids, sugars, ketones, aldehydes, carboxylic acids, and amides) play a key role in the crystalline formation of these metal-NPs [46,47]. Moreover, the concentration of these organic compounds can vary in concentration depending on the plant species and extraction method and even the growth stage and environmental conditions [48]. In our research, white tea (*Camellia sinensis*) was selected due to its remarkably high content of polyphenols, which potentially act as reducing and capping agents [14]. Green synthesis methods in aqueous solutions are commonly carried out under mild reaction conditions and with longer reaction times to ensure complete reduction of the metal ions and to precisely control the size and morphology of the metal-NPs at the end of the reaction. During the precipitation reaction, the reduction of Ag^{+} to Ag^{0} occurred immediately after the $AgNO_3$ dissolution in the white tea extract. The possible mechanism of Ag^{+} reduction involves the ionisation of the polyphenols, resulting in the reduction of Ag ions as the tea polyphenols are oxidised to quinone [14]. Experimentally, the reduction process leading to the WT_AgNPs formation was indicated by the color change of the suspension from yellow to brown [35].

Our results demonstrated that the white tea extract effectively acted as a reducing and stabilising agent for the different synthesised WT_AgNPs, showing an average spherical size ~20 nm. Previous research employing different plant extracts (v.gr., *Aloe vera*, *Drosera ittatee*, *Ephedra procera*) have produced similar particle sizes and morphologies to those obtained in the current study [17]. In addition, the three different WT_AgNPs presented a characteristic gray-core wrapped (Fig. 3), attributed to the presence of organic content derived from white tea synthesis processes [35]. The presence of these organic compounds (i.e., tannins, polyphenols, and flavonoids) in all silver nanoparticles was also confirmed by identifying their specific molecular groups (shown in the ATR-FTIR results) [14,21]. Moreover, WT_AgNPs_CHS showed a characteristic absorption peak in the IR spectrum (position at 616 cm^{-1}), evidencing the CHS interaction with the nanoparticles during their functionalisation [43,49]. The organic content determined by thermogravimetric analysis corroborated the occurrence of these chemical components from the WT solutions [50], being slightly higher with the incorporation of CHS. This reaction occurs between the amino ($-NH_2$) and hydroxyl (-OH) groups of the CHS structure with the metal ion solution, forming metal-chitosan complexes or adsorbing them on the surface of the NPs [51,52]. Multiple mechanisms, including ion exchange, chelation, and surface adsorption, play a key role in the formation of CHS functionalised AgNPs, influencing their crystalline properties such as crystal size, shape and/or particle aggregation [27]. Moreover, the presence and chemical modification of CHS by various processes has also proven to be useful in modifying the compositional and biocompatibility properties of functionalised chitosan-NPs targeting different biomedical applications (e.g. drug delivery [53]). On the other hand, fluoride ions can also influence the crystal size, shape, and

dispersity of metal-NPs synthesised via precipitation method. In addition, fluoride can also adsorb into the NPs surface, influencing their surface energy and reactivity [54]. Our study shows that fluoride functionalization provide stability and prevent aggregation of AgNPs, influencing their homogeneous response in potential biomedical application (i.e., preventing dental caries) [12].

Moreover, the crystal identification for all the WT_AgNPs (Fig. 2) corresponded to Ag^0 face-centred cubic (FCC) structure [55], showing similar crystallite size values (approximately ~22 nm, related to the average crystal domains). Overall, these results demonstrated the formation of a homogeneous single-phase Ag crystallisation with compositional and crystalline characteristics controlled by the reducing ability of the white tea extract during nanoparticle synthesis. The uniform spherical shape and reduced size of the WT_AgNPs significantly enhances the surface-to-volume ratio and enable homogeneous reactivity in their potential applications, e.g. antibacterial properties [37]. A previous study has also found that AgNPs exhibit a shape-dependent interaction with different type of bacteria (in particular, *Staphylococcus aureus*, *Pseudomonas aeruginosa*) [56]. Moreover, the diameter size of the synthetized WT_AgNPs (as single crystals or aggregates) allows for a higher diffusion capacity through the dentinal tubule, fostering their different capabilities and uses in different dental applications [57,58].

Carious lesions comprehend a scale from initial loss of minerals at the ultrastructural/nanoscale level to total tooth destruction [59]. Early visible signs of caries consist of non-cavitated coronal or root carious lesions, expressed by tissue demineralization (i.e., dissolution of hydroxyapatite crystals). The process of mineral alteration caused by caries results in a modification of the structural and chemical composition of the dental tissue, leading to a consequent alteration of its mechanical properties. As the lesion progresses into the dentine, further mineral loss and collagen degrades, resulting in cavitation [60]. The caries process is a continuum resulting from many cycles of demineralization and remineralization [61]. Our study observed a significant difference in the relative amount of mineral phosphate to the organic matrix (degree of mineralisation, ATR-FTIR analyses) in the DD group, indicating that demineralisation has occurred successfully by means pH-cycling method [62,63]. The application of the different WT_AgNPs treatments provoked a significant increase in the degree of mineralisation content compared to the DD group. These effects can be partially attributed to the remineralising capacity of the fluoride ions presented in the composition of the white tea extracts (3.2 mg/kg to 400 mg/kg by weight in dry samples) [64]. Moreover, the presence of Ca complexes from the carboxyl derivatives/reactive groups in plant polyphenols - with a potential chelating effect - can react with phosphate groups to initiate HAp formation [65]. In addition, the stabilising action on the collagen network combined with incorporating biomolecules from the organic compounds of the WT can also promote dentine remineralisation [66]. On the other hand, chitosan has demonstrated to induce significant CaP deposition on demineralised dentine by promoting crystal nucleation [19]. In our results, the NaF functionalisation of the nanoparticles showed the highest degree of mineralisation values, even greater than SD. Fluoride is the mainstay of remineralisation in dentistry; it has been shown to inhibit the demineralisation of hydroxyapatite crystals [39]. Regarding the CI obtained by ATR-FTIR, the differential dissolution of non-apatitic domains compared to apatitic environments of higher crystallinity was observed, as previously reported during the pH-cycling procedure [37]. For the WT_AgNPs application groups, a relative incorporation of phosphates with different degrees of crystallinity at the molecular level was suggested, increasing the CI values compared to SD. Furthermore, XRD results showed an increase in the HAp crystallite sizes of the WT_AgNPs experimental groups, reaching values similar to SD. This effect on the crystal perfection may be due to the ability of Ag^+ ions to modify the HAp crystalline environment, occupying either a lattice site or an interstitial site depending on the amount of Ag^+ incorporated [67]. Moreover, the alteration of the crystallite size may be due to processes mediated by ionic complexation of the organic substances from the white tea, as previously discussed.

Applying the synthetised WT_AgNPs in the demineralised dentine evidenced different distribution patterns on the dentine surface and filling of the dentine tubules related to the degree of aggregation of the spherical nanoparticles. In this regard, plant extracts have proven to help control morphology and overcome the agglomeration setback during the synthesis of a wide range of particles [68,69]. The effect of the WT_AgNPs application on the physicochemical and microstructural properties of the dentine surface resulted in a modification of the mechanical response of the demineralised dentine. These overall changes would yield mechanical properties comparable to sound dentine and indicate successful functional remineralisation of the tooth structure. Notably, our mechanical results revealed a significant increase in the dentine flexural strength of the WT_AgNPs application groups compared to the DD and even overcoming the SD values. This effect on the dentine strength is related to the increase in the degree of mineralisation and crystalline properties of HAp combined with the possible modification of collagen matrix properties in the tooth structure. The collagen matrix influenced the structural features of apatite at the atomic scale, controlling the size and dimensional distribution at a larger scale in mineralised tissues [70]. Previous authors have suggested that the conjugation of collagen with AgNPs leads to a compact aggregate, mainly producing modification in the different types of secondary protein structures (e.g., α-helix and β-sheet) [71]. In addition, phenolic compounds present in green tea (i.e. EGG, EGC, ECG, EG) are a natural collagen cross-linking agent capable of improving the mechanical properties of dentine, as well as reducing its biodegradability against host-derived metalloproteinases (MTTs) [47,48]. Moreover, the effects of NaF on the demineralisation of dental hard tissues and the improvement of its remineralisation are well established [72–74]. It has also been demonstrated that chitosan could increase the number of crosslinks between collagen fibres and neutralise MTTs from the dentine [75]. Overall, the mechanical response of the WT_AgNPs dentine samples was enhanced by the effects on the organic matrix of the different natural compounds present both in the white tea and in the chitosan functionalisation, and the increase in the dentine mineralisation by different processes of crystalline formation and alteration described above.

The AgNPs synthesis by chemical methods in Dentistry are widely known, however the use of organic compounds (e.g. extracted from white tea) for their reduction offers a more natural and environmentally friendly alternative. This study provides an easy, reproducible, and effective method mediated by green chemistry, obtaining particular physico-chemical WT_AgNPs properties. The advantages of using plant extracts for green synthesis are energy efficiency, cost-effectiveness, protection of human health and the environment, resulting in less waste and safer products. Moreover, the application of these WT_AgNPs does not form black silver chloride layers on the dentine surface, thus avoiding the undesired aesthetic effect of dental products that usually contain silver nitrate (e.g. silver diamine fluoride) [74,76]. Following the findings our results, the WT_AgNPs present a significant potential to be utilized in oral care products and dental materials to manage caries process (i.e., mouthwashes, dentifrices, varnishes, remineralising solutions) and lesions (i.e., sealants, infiltrates, adhesives, resin composites, glass ionomers, etc.) [77]. Also, previous studies have shown that the infiltration capacity resin modified with AgNPs addition was not negatively affected in enamel proximal caries [78]. Based on these findings, it seems reasonable to assume that the antibacterial effects of dental materials incorporating AgNP should prevent secondary caries. Further studies are needed to evaluate the integration and interaction of these WT_AgNPs with materials commonly used in clinical practice and their possible combined effect (i.e., adhesives, composite resins). However, some of the limitations in the synthesis of metal-NPs, also presented in the current research, are related to the control of the crystal size and NPs aggregation properties by modifying the reaction conditions, and how

these characteristics may compromise their efficacy and antimicrobial capacity as well as modify their cytotoxicity.

5. Conclusions

In this study, a one-step green synthesis of stable silver nanoparticles using white tea (*Camellia sinensis*) extract and functionalised with CHS and NaF is presented. The proposed green synthesis was efficient in the reduction reaction and stability of the synthesised AgNPs, obtaining spherical morphologies with an average crystal size of ~20 nm and different degrees of aggregation. The application of WT_AgNPs on demineralised dentin (obtained by pH cycling procedure) resulted in an enhancement in the degree of mineralisation and increase in the crystallite size of the dentine apatite. The mechanical strength of the dentine with the application of the different WT_AgNPs increased compared to the sound and demineralised control groups. This sustainable method could be an alternative to conventional methods used for the synthesis of silver nanoparticles especially for the management of caries disease.

Funding

This work was supported by the Spanish Ministry of Economy and Competitiveness [grant number PID2020-116660GB-I00, RNM-408-UGR20], and the European Regional Development Fund (ERDF) - Next Generation/EU program.

Declaration of competing interest

The authors declare the following financial interests/personal relationships which may be considered as potential competing interests: Pedro Alvarez-lloret reports financial support was provided by Spanish Ministry of Economy and Competitiveness. Pedro Alvarez-lloret reports a relationship with University of Oviedo that includes: funding grants. If there are other authors, they declare that they have no known competing financial interests or personal relationships that could have appeared to influence the work reported in this paper.

Acknowledgments

The authors would like to thank the staff of CIC (UGR, Spain) and SCT (UNIOVI, Spain) for providing technical support and Yudi Gómez Villaescusa for assisting in the sample preparation.

References

[1] S. Medici, M. Peana, V.M. Nurchi, M.A. Zoroddu, Medical uses of silver: history, myths, and scientific evidence, J. Med. Chem. 62 (2019) 5923–5943, https://doi.org/10.1021/acs.jmedchem.8b01439.
[2] M.L. Mei, E.C.M. Lo, C.H. Chu, Arresting dentine caries with silver diamine fluoride: what's behind it? J. Dent. Res. 97 (2018) 751–758, https://doi.org/10.1177/0022034518774783.
[3] V. MacHiulskiene, G. Campus, J.C. Carvalho, I. Dige, K.R. Ekstrand, A. Jablonski-Momeni, M. Maltz, D.J. Manton, S. Martignon, E.A. Martinez-Mier, N.B. Pitts, A. G. Schulte, C.H. Splieth, L.M.A. Tenuta, A. Ferreira Zandona, B. Nyvad, Terminology of dental caries and dental caries management: consensus report of a workshop organized by ORCA and Cariology Research Group of IADR, Caries Res. 54 (2020) 7–14, https://doi.org/10.1159/000503309.
[4] L.M.A. Tenuta, J.A. Cury, Fluoride: its role in dentistry, Braz. Oral Res. 24 (2010) 9–17, https://doi.org/10.1590/S1806-83242010000500003.
[5] R.Z. LeGeros, Chemical and crystallographic events in the caries process, J. Dent. Res. 69 (1990) 567–574, https://doi.org/10.1177/00220345900690s113.
[6] M.K. Arifa, R. Ephraim, T. Rajamani, Recent advances in dental hard tissue remineralization: a review of literature, Int. J. Clin. Pediatr. Dent. 12 (2019) 139–144, https://doi.org/10.5005/jp-journals-10005-1603.
[7] N. Preethi P, Remineralizing agent-then and now-an update, Dentistry 04 (2014) 2–6, https://doi.org/10.4172/2161-1122.1000256.
[8] F. Bertoglio, L. de Vita, A. D'Agostino, Y.D. Fernandez, A. Falqui, A. Casu, D. Merli, C. Milanese, S. Rossi, A. Taglietti, L. Visai, P. Pallavicini, Increased antibacterial and antibiofilm properties of silver nanoparticles using silver fluoride as precursor, Molecules 25 (2020), https://doi.org/10.3390/molecules25153494.
[9] J.A. Teixeira, A.V. Costa E Silva, V.E. Dos Santos, P.C. De Melo, M. Arnaud, M. G. Lima, M.A.P. Flores, T.C.M. Stamford, J.R.D. Pereira, A.G.R. Targino, A. Galembeck, A. Rosenblatt, Effects of a new nano-silver fluoride-containing dentifrice on demineralization of enamel and Streptococcus mutans adhesion and acidogenicity, Int. J. Dent. 2018 (2018), https://doi.org/10.1155/2018/1351925.
[10] B.A. Aldhaian, A.A. Balhaddad, A.A. Alfaifi, J.A. Levon, G.J. Eckert, A.T. Hara, F. Lippert, In vitro demineralization prevention by fluoride and silver nanoparticles when applied to sound enamel and enamel caries-like lesions of varying severities, J. Dent. 104 (2021) 103536, https://doi.org/10.1016/j.jdent.2020.103536.
[11] F.A. Dias, C.M.P. Vidal, C.L. Comnick, X.J. Xie, S.B. Berger, Effect of silver nanoparticles associated with fluoride on the progression of root dentin caries in vitro, PLoS One 18 (2023) 1–16, https://doi.org/10.1371/journal.pone.0277275.
[12] E. Kemnitz, S. Mahn, T. Krahl, Nano metal fluorides: small particles with great properties, ChemTexts 6 (2020) 1–27, https://doi.org/10.1007/s40828-020-00115-w.
[13] E. Kemnitz, Nanoscale metal fluorides: a new class of heterogeneous catalysts, Catal, Sci. Technol. 5 (2015) 786–806, https://doi.org/10.1039/c4cy01397b.
[14] W.R. Rolim, M.T. Pelegrino, B. de Araújo Lima, L.S. Ferraz, F.N. Costa, J. S. Bernardes, T. Rodigues, M. Brocchi, A.B. Seabra, Green tea extract mediated biogenic synthesis of silver nanoparticles: characterization, cytotoxicity evaluation and antibacterial activity, Appl. Surf. Sci. 463 (2019) 66–74, https://doi.org/10.1016/j.apsusc.2018.08.203.
[15] S. Jain, N. Saxena, M.K. Sharma, S. Chatterjee, Metal nanoparticles and medicinal plants: present status and future prospects in cancer therapy, Mater. Today Proc. 31 (2019) 662–673, https://doi.org/10.1016/j.matpr.2020.06.602.
[16] S. Some, B. Sarkar, K. Biswas, T.K. Jana, D. Bhattacharjya, P. Dam, R. Mondal, A. Kumar, A.K. Deb, A. Sadat, S. Saha, A. Kati, A. Kati, I. Ocsoy, O.L. Franco, A. Mandal, S. Mandal, A.K. Mandal, İ.A. İnce, Bio-molecule functionalized rapid one-pot green synthesis of silver nanoparticles and their efficacy toward the multidrug resistant (MDR) gut bacteria of silkworms (Bombyx mori), RSC Adv. 10 (2020) 22742–22757, https://doi.org/10.1039/d0ra03451g.
[17] M. Goel, A. Sharma, B. Sharma, Recent advances in biogenic silver nanoparticles for their biomedical applications, Sustain. Chem. 4 (2023) 61–94, https://doi.org/10.3390/suschem4010007.
[18] M. Forough, F. Khalil, Biological and green synthesis of silver nanoparticles, Turkish J. Eng, Environ. Sci. 34 (2010) 281–287, https://doi.org/10.3906/muh-1005-30.
[19] L. Liu, Z. Zhang, L. Cao, Z. Xiong, Y. Tang, Y. Pan, Cytotoxicity of phytosynthesized silver nanoparticles: a meta-analysis by machine learning algorithms, Sustain. Chem. Pharm. 21 (2021) 100425, https://doi.org/10.1016/j.scp.2021.100425.
[20] H. Chandra, P. Kumari, E. Bontempi, S. Yadav, Medicinal plants: treasure trove for green synthesis of metallic nanoparticles and their biomedical applications, Biocatal. Agric. Biotechnol. 24 (2020) 101518, https://doi.org/10.1016/j.bcab.2020.101518.
[21] S. Liao, Y. Tang, C. Chu, W. Lu, B. Baligen, Y. Man, Y. Qu, Application of green tea extracts epigallocatechin-3-gallate in dental materials: recent progress and perspectives, J. Biomed. Mater. Res. - Part A. 108 (2020) 2395–2408, https://doi.org/10.1002/jbm.a.36991.
[22] P. Jose, K. Sanjeev, M. Sekar, Effect of green and white tea pretreatment on remineralization of demineralized dentin by CPP-ACFP-an invitro microhardness analysis, J. Clin. Diagn. Res. 10 (2016) ZC85–ZC89, https://doi.org/10.7860/JCDR/2016/16038.7674.
[23] I.S. Zhao, S.S. Gao, N. Hiraishi, M.F. Burrow, D. Duangthip, M.L. Mei, E.C.M. Lo, C. H. Chu, Mechanisms of silver diamine fluoride on arresting caries: a literature review, Int. Dent. J. 68 (2018) 67–76, https://doi.org/10.1111/idj.12320.
[24] F.A. Curylofo-Zotti, A.C. Tedesco, G.T.C. Lizarelli, L.A.U. Takahashi, S.A. M. Corona, Effect of green tea-loaded chitosan nanoparticles on leathery dentin microhardness, Odontology 109 (2021) 860–867, https://doi.org/10.1007/s10266-021-00611-6.
[25] M.A. Mohammed, J.T.M. Syeda, K.M. Wasan, E.K. Wasan, An overview of chitosan nanoparticles and its application in non-parenteral drug delivery, Pharmaceutics 9 (2017) 53, https://doi.org/10.3390/pharmaceutics9040053.
[26] I.X. Yin, J. Zhang, I.S. Zhao, M.L. Mei, Q. Li, C.H. Chu, The antibacterial mechanism of silver nanoparticles and its application in dentistry, Int. J. Nanomedicine 15 (2020) 2555–2562, https://doi.org/10.2147/IJN.S246764.
[27] T.T.V. Phan, D.T. Phan, X.T. Cao, T.C. Huynh, J. Oh, Roles of chitosan in green synthesis of metal nanoparticles for biomedical applications, Nanomaterials 11 (2021) 1–15, https://doi.org/10.3390/nano11020273.
[28] M. Venkatesham, D. Ayodhya, A. Madhusudhan, N. Veera Babu, G. Veerabhadram, A novel green one-step synthesis of silver nanoparticles using chitosan: catalytic activity and antimicrobial studies, Appl. Nanosci. 4 (2014) 113–119, https://doi.org/10.1007/s13204-012-0180-y.
[29] S.H.S. Dananjaya, R.M.C. Udayangani, C. Oh, C. Nikapitiya, J. Lee, M. De Zoysa, Green synthesis, physio-chemical characterization and anti-candidal function of a biocompatible chitosan gold nanocomposite as a promising antifungal therapeutic agent, RSC Adv. 7 (2017) 9182–9193, https://doi.org/10.1039/c6ra26915j.
[30] M. Potara, D. Maniu, S. Astilean, The synthesis of biocompatible and SERS-active gold nanoparticles using chitosan, Nanotechnology 20 (2009), https://doi.org/10.1088/0957-4484/20/31/315602.
[31] L. Biao, S. Tan, Y. Wang, X. Guo, Y. Fu, F. Xu, Y. Zu, Z. Liu, Synthesis, characterization and antibacterial study on the chitosan-functionalized Ag nanoparticles, Mater. Sci. Eng. C 76 (2017) 73–80, https://doi.org/10.1016/j.msec.2017.02.154.
[32] M.A. Asghar, R.I. Yousuf, M.H. Shoaib, M.A. Asghar, Antibacterial, anticoagulant and cytotoxic evaluation of biocompatible nanocomposite of chitosan loaded green synthesized bioinspired silver nanoparticles, Int. J. Biol. Macromol. 160 (2020) 934–943, https://doi.org/10.1016/j.ijbiomac.2020.05.197.

[33] Y. Gao, Y. Wu, Recent advances of chitosan-based nanoparticles for biomedical and biotechnological applications, Int. J. Biol. Macromol. 203 (2022) 379–388, https://doi.org/10.1016/j.ijbiomac.2022.01.162.
[34] E. Fakhri, H. Eslami, P. Maroufi, F. Pakdel, S. Taghizadeh, K. Ganbarov, M. Yousefi, A. Tanomand, B. Yousefi, S. Mahmoudi, H.S. Kafil, Chitosan biomaterials application in dentistry, Int. J. Biol. Macromol. 162 (2020) 956–974, https://doi.org/10.1016/j.ijbiomac.2020.06.211.
[35] M. Zargar, K. Shameli, G.R. Najafi, F. Farahani, Plant mediated green biosynthesis of silver nanoparticles using Vitex negundo L. extract, J. Ind. Eng. Chem. 20 (2014) 4169–4175, https://doi.org/10.1016/j.jiec.2014.01.016.
[36] P. Senthilkumar, G. Yaswant, S. Kavitha, E. Chandramohan, G. Kowsalya, R. Vijay, B. Sudhagar, D.S.R.S. Kumar, Preparation and characterization of hybrid chitosan-silver nanoparticles (Chi-Ag NPs); a potential antibacterial agent, Int. J. Biol. Macromol. 141 (2019) 290–297, https://doi.org/10.1016/j.ijbiomac.2019.08.234.
[37] P.L.L. Freire, A.J.R. Albuquerque, I.A.P. Farias, T.G. da Silva, J.S. Aguiar, A. Galembeck, M.A.P. Flores, F.C. Sampaio, T.C.M. Stamford, A. Rosenblatt, Antimicrobial and cytotoxicity evaluation of colloidal chitosan – silver nanoparticles – fluoride nanocomposites, Int. J. Biol. Macromol. 93 (2016) 896–903, https://doi.org/10.1016/j.ijbiomac.2016.09.052.
[38] M. Marquezan, F.N.P. Corrêa, M.E. Sanabe, L.E. Rodrigues Filho, J. Hebling, A. C. Guedes-Pinto, F.M. Mendes, Artificial methods of dentine caries induction: a hardness and morphological comparative study, Arch. Oral Biol. 54 (2009) 1111–1117, https://doi.org/10.1016/j.archoralbio.2009.09.007.
[39] V.T. Noronha, A.J. Paula, G. Durán, A. Galembeck, K. Cogo-Müller, M. Franz-Montan, N. Durán, Silver nanoparticles in dentistry, Dent. Mater. 33 (2017) 1110–1126, https://doi.org/10.1016/j.dental.2017.07.002.
[40] C. de C.ALopes, P.H.J.O. Limirio, V.R. Novais, P. Dechichi, Fourier transform infrared spectroscopy (FTIR) application chemical characterization of enamel, dentin and bone, Appl. Spectrosc. Rev. 53 (2018) 747–769, https://doi.org/10.1080/05704928.2018.1431923.
[41] A.B. Rodriguez-Navarro, C.S. Romanek, P. Alvarez-Lloret, K.F. Gaines, Effect of in ovo exposure to PCBs and Hg on clapper rail bone mineral chemistry from a contaminated salt marsh in coastal Georgia, Environ. Sci. Technol. 40 (2006) 4936–4942, https://doi.org/10.1021/es060769x.
[42] K. Shameli, M. Bin Ahmad, E.A. Jaffar Al-Mulla, N.A. Ibrahim, P. Shabanzadeh, A. Rustaiyan, Y. Abdollahi, S. Bagheri, S. Abdolmohammadi, M.S. Usman, M. Zidan, Green biosynthesis of silver nanoparticles using callicarpa maingayi stem bark extraction, Molecules 17 (2012) 8506–8517, https://doi.org/10.3390/molecules17078506.
[43] S. Anusuya, K.N. Banu, Silver-chitosan nanoparticles induced biochemical variations of chickpea (Cicer arietinum L.), Biocatal. Agric. Biotechnol. 8 (2016) 39–44, https://doi.org/10.1016/j.bcab.2016.08.005.
[44] S. Si, T.K. Mandal, Tryptophan-based peptides to synthesize gold and silver nanoparticles: a mechanistic and kinetic study, Chem. - A Eur. J. 13 (2007) 3160–3168, https://doi.org/10.1002/chem.200601492.
[45] D. Nath, P. Banerjee, Green nanotechnology - a new hope for medical biology, Environ. Toxicol. Pharmacol. 36 (2013) 997–1014, https://doi.org/10.1016/j.etap.2013.09.002.
[46] J. Singh, T. Dutta, K.H. Kim, M. Rawat, P. Samddar, P. Kumar, “Green” synthesis of metals and their oxide nanoparticles: applications for environmental remediation, J. Nanobiotechnology. 16 (2018) 1–24, https://doi.org/10.1186/s12951-018-0408-4.
[47] S. Iravani, Green synthesis of metal nanoparticles using plants, Green Chem. 13 (2011) 2638–2650, https://doi.org/10.1039/c1gc15386b.
[48] C. Hano, B.H. Abbasi, Plant-based green synthesis of nanoparticles: production, characterization and applications, Biomolecules 12 (2022) 1–9, https://doi.org/10.3390/biom12010031.
[49] P. Gupta, M. Bajpai, S.K. Bajpai, Textile technology: investigation of antibacterial properties of silver nanoparticle-loaded poly (acrylamide-co-itaconic acid)-grafted cotton fabric, J. Cotton Sci. 12 (2008) 280–286.
[50] S. Elfersi, G. Grégoire, P. Sharrock, Characterization of sound human dentin particles of sub-millimeter size, Dent. Mater. 18 (2002) 529–534, https://doi.org/10.1016/S0109-5641(01)00085-9.
[51] L.A. Frank, G.R. Onzi, A.S. Morawski, A.R. Pohlmann, S.S. Guterres, R.V. Contri, Chitosan as a coating material for nanoparticles intended for biomedical applications, React. Funct. Polym. 147 (2020) 104459, https://doi.org/10.1016/j.reactfunctpolym.2019.104459.
[52] M. Collado-González, M.G. Montalbán, J. Peña-García, H. Pérez-Sánchez, G. Víllora, F.G. Díaz Baños, Chitosan as stabilizing agent for negatively charged nanoparticles, Carbohydr. Polym. 161 (2017) 63–70, https://doi.org/10.1016/j.carbpol.2016.12.043.
[53] J. Zhang, W. Xia, P. Liu, Q. Cheng, T. Tahirou, W. Gu, B. Li, Chitosan modification and pharmaceutical/biomedical applications, Mar. Drugs 8 (2010) 1962–1987, https://doi.org/10.3390/md8071962.
[54] M.Z.I. Nizami, V.W. Xu, I.X. Yin, O.Y. Yu, C.H. Chu, Metal and metal oxide nanoparticles in caries prevention: a review, Nanomaterials 11 (2021), https://doi.org/10.3390/nano11123446.
[55] V. Ahluwalia, S. Elumalai, V. Kumar, S. Kumar, R.S. Sangwan, Nano silver particle synthesis using Swertia paniculata herbal extract and its antimicrobial activity, Microb. Pathog. 114 (2018) 402–408, https://doi.org/10.1016/j.micpath.2017.11.052.
[56] J.Y. Cheon, S.J. Kim, Y.H. Rhee, O.H. Kwon, W.H. Park, Shape-dependent antimicrobial activities of silver nanoparticles, Int. J. Nanomedicine 14 (2019) 2773–2780, https://doi.org/10.2147/IJN.S196472.
[57] S. Arslan, S. Ekrikaya, N. Ildiz, S. Yusufbeyoglu, İ. Ocsoy, Evaluation of the antibacterial activity of dental adhesive containing biogenic silver nanoparticles decorated nanographene oxide nanocomposites (Ag@nGO NCs) and effect on bond strength to dentine, Odontology 112 (2024) 341–354, https://doi.org/10.1007/s10266-023-00836-7.
[58] T. Aslan, Ş. Dadi, O. Kafdag, N. Temur, N. Ildiz, I. Ocsoy, Y. Ustun, Rational design of EDTA-incorporated nanoflowers as novel and effective endodontic disinfection against biofilms, Odontology 112 (2024) 444–452, https://doi.org/10.1007/s10266-023-00857-2.
[59] A.M. Kielbassa, J. Muller, C.R. Gernhardt, Closing the gap between oral hygiene and minimally invasive dentistry: a review on the resin infiltration technique of incipient (proximal) enamel lesions, Quintessence Int. 40 (2009) 663–681.
[60] R.L. Slayton, O. Urquhart, M.W.B. Araujo, M. Fontana, S. Guzmán-Armstrong, M. M. Nascimento, B.B. Nový, N. Tinanoff, R.J. Weyant, M.S. Wolff, D.A. Young, D. T. Zero, M.P. Tampi, L. Pilcher, L. Banfield, A. Carrasco-Labra, Evidence-based clinical practice guideline on nonrestorative treatments for carious lesions: a report from the American Dental Association, J. Am. Dent. Assoc. 149 (2018) 837–849.e19, https://doi.org/10.1016/j.adaj.2018.07.002.
[61] D.J. Epasinghe, C.K.Y. Yiu, M.F. Burrow, Effect of flavonoids on remineralization of artificial root caries, Aust. Dent. J. 61 (2016) 196–202, https://doi.org/10.1111/adj.12367.
[62] J.S. Zuluaga-Morales, M.V. Bolaños-Carmona, C.C. Cifuentes-Jiménez, P. Álvarez-Lloret, Chemical, microstructural and morphological characterisation of dentine caries simulation by pH-cycling, Minerals 12 (2021) 5, https://doi.org/10.3390/min12010005.
[63] J.S. Zuluaga-Morales, M.V. Bolaños-Carmona, P., Álvarez-Lloret, pH-cycling, dynamic chemical model in dentine caries creation. A systematic review and meta-analysis, Int. J. Med. Dent. 26 (2022) 585–608.
[64] S. Rohym, Effect of green tea, stevia extract solutions, and fluoride-based mouthwash on remineralization of incipient enamel lesion: an in vitro study., Ahram Can, Dent. J. 2 (2023) 13–25, https://doi.org/10.21608/acdj.2023.281310.
[65] K. Alorku, M. Manoj, A. Yuan, A plant-mediated synthesis of nanostructured hydroxyapatite for biomedical applications: a review, RSC Adv. 10 (2020) 40923–40939, https://doi.org/10.1039/d0ra08529d.
[66] H. Farouk, R. Mosallam, N. Aidaros, Effect of green tea, black tea and Moringa oleifera on remineralization of artificially demineralized enamel and dentin: an in-vitro microhardness analysis, Adv. Dent. J. 3 (2021) 24–34, https://doi.org/10.21608/adjc.2020.34873.1072.
[67] M. Riaz, R. Zia, A. Ijaz, T. Hussain, M. Mohsin, A. Malik, Synthesis of monophasic Ag doped hydroxyapatite and evaluation of antibacterial activity, Mater. Sci. Eng. C 90 (2018) 308–313, https://doi.org/10.1016/j.msec.2018.04.076.
[68] Z. Xiao, M. Yuan, B. Yang, Z. Liu, J. Huang, D. Sun, Plant-mediated synthesis of highly active iron nanoparticles for Cr (VI) removal: investigation of the leading biomolecules, Chemosphere 150 (2016) 357–364, https://doi.org/10.1016/j.chemosphere.2016.02.056.
[69] M.M. Alves, S.M. Andrade, L. Grenho, M.H. Fernandes, C. Santos, M.F. Montemor, Influence of apple phytochemicals in ZnO nanoparticles formation, photoluminescence and biocompatibility for biomedical applications, Mater. Sci. Eng. C 101 (2019) 76–87, https://doi.org/10.1016/j.msec.2019.03.084.
[70] Y. Wang, T. Azaïs, M. Robin, A. Vallée, C. Catania, P. Legriel, G. Pehau-Arnaudet, F. Babonneau, M.M. Giraud-Guille, N. Nassif, The predominant role of collagen in the nucleation, growth, structure and orientation of bone apatite, Nat. Mater. 11 (2012) 724–733, https://doi.org/10.1038/nmat3362.
[71] M. Drobota, I. Grierosu, I. Radu, D.S. Vasilescu, The effect of silver nanoparticles on the collagen secondary structure, Key Eng. Mater. 638 (2015) 8–13, https://doi.org/10.4028/www.scientific.net/KEM.638.8.
[72] O.Y. Yu, M.L. Mei, I.S. Zhao, Q.L. Li, E.C.M. Lo, C.H. Chu, Remineralisation of enamel with silver diamine fluoride and sodium fluoride, Dent. Mater. 34 (2018) e344–e352, https://doi.org/10.1016/j.dental.2018.10.007.
[73] D. Duangthip, M.C.M. Wong, C.H. Chu, E.C.M. Lo, Caries arrest by topical fluorides in preschool children: 30-month results, J. Dent. 70 (2018) 74–79, https://doi.org/10.1016/j.jdent.2017.12.013.
[74] I.S. Zhao, I.X. Yin, M.L. Mei, E.C.M. Lo, J. Tang, Q. Li, L.Y. So, C.H. Chu, Remineralising dentine caries using sodium fluoride with silver nanoparticles: an in vitro study, Int. J. Nanomedicine 15 (2020) 2829–2839, https://doi.org/10.2147/IJN.S247550.
[75] S.B. Nimbeni, B.S. Nimbeni, D.D. Divakar, Role of chitosan in remineralization of enamel and dentin: a systematic review, Int. J. Clin. Pediatr. Dent. 14 (2021) 562–568, https://doi.org/10.5005/jp-journals-10005-1971.
[76] I.X. Yin, O.Y. Yu, I.S. Zhao, M.L. Mei, Q.L. Li, J. Tang, E.C.M. Lo, C.H. Chu, Inhibition of dentine caries using fluoride solution with silver nanoparticles: an in vitro study, J. Dent. 103 (2020) 103512, https://doi.org/10.1016/j.jdent.2020.103512.
[77] A. Banerjee, C. Splieth, L. Breschi, M. Fontana, S. Paris, M. Burrow, F. Crombie, L. Foster Page, P. Gatón-Hernández, R.A. Giacaman, N. Gugnani, R. Hickel, R. A. Jordan, S. Leal, E. Lo, H. Tassery, W.M. Thomson, D.J. Manton, F. Schwendicke, When to intervene in the caries process? A Delphi consensus statement, Br. Dent. J. 229 (2020) 474–482, https://doi.org/10.1038/s41415-020-2220-4.
[78] A.M. Kielbassa, M.R. Leimer, J. Hartmann, S. Harm, M. Pasztorek, I.B. Ulrich, Ex vivo investigation on internal tunnel approach/internal resin infiltration and external nanosilver-modified resin infiltration of proximal caries exceeding into dentin, PLoS One 15 (2020) 1–22, https://doi.org/10.1371/journal.pone.0228249.